

# Confotronic Dynamics of Tubular Lattices

Osman Kahraman<sup>1</sup>, Hervé Mohrbach<sup>1,2</sup>, Martin Michael Müller<sup>1,2</sup>, Igor M. Kulić<sup>2</sup>

<sup>1</sup>*Equipe BioPhysStat, ICPMB-FR CNRS 2843, Université de Lorraine; 1 boulevard Arago, 57070 Metz, France and*

<sup>2</sup>*CNRS, Institut Charles Sadron; 23 rue du Loess BP 84047, 67034 Strasbourg, France*

(Dated: March 21, 2022)

Tubular lattices are ubiquitous in nature and technology. Microtubules and nanotubes of all kinds act as important pillars of biological cells and the man-made nano-world. We show that when prestress is introduced in such structures, localized conformational quasiparticles emerge and govern the collective shape dynamics of the lattice. When coupled *via* cooperative interactions these quasiparticles form larger-scale quasipolymer superstructures exhibiting collective dynamic modes and giving rise to a hallmark behavior radically different from semiflexible beams.

PACS numbers: 87.16.aj,82.35.Pq,87.15.-v

## I. INTRODUCTION

Tubular and cylindrical lattices are abundant in living nature and give rise to important filamentous structures, such as bacterial flagella and microtubules. Inspired by biology, nanotubes made from various building blocks like carbon [1], DNA [2] or amphiphilic molecules [3, 4] have been synthesized. Remarkably, in the presence of internal prestress, almost all of these tubular objects can adopt superhelical structures, *i.e.*, tubes whose centerline describes a large-scale helix in space. Superhelical carbon nanotubes with micron-meter size pitch have been observed [5] and their elastic properties probed [6]. It is believed that their coiling results from the periodic arrangement of defects (pairs of heptagon-pentagon rings) in the hexagonal carbon lattice forming the wall of the tube [7]. DNA nanotubes [8] adsorbed on a substrate resemble squeezed helices indicating that they assume a three-dimensional superhelical structure under free conditions [9]. Supramolecular chiral helical nanofibers made of self-assembling lipids have been synthesized. It was shown that the torsional stress, created by the steric interactions of the chemical groups at the surface of the tube, causes the nanofibers to coil into a superhelix that minimizes the internal prestress [10]. In bacterial flagella and microtubules the coexistence of several conformational states of their individual constituents is in elastic conflict with their lattice geometry, resulting in prestresses that can be minimized by forming superhelical shapes [11–13]. The protein monomer units of bacterial flagella are arranged in eleven protofilaments parallel to the centerline that can switch from a short to a longer state and can slide down relative to their lateral neighbors creating local twist and curvature [11]. In a similar manner, the wall of microtubules is made of protofilaments built by the polymerization of tubulin dimers. There are experimental indications that the tubulin dimers can indeed switch between straight and curved conformational states in the presence of taxol [14] and display an allosteric cooperative interaction along their protofilaments' axes [15]. The integrity of the tubular lattice can be maintained either by forcing all protofilaments in their straight state or by creating a mixed phase with a cluster of curved protofil-

aments while the rest of the protofilaments stays in their straight state. When this phase is energetically more favorable, the microtubule bends in the direction of the block formed by the curved protofilaments. Since microtubules have internal twist [16] (*i.e.*, the protofilaments are not parallel to the centerline of the tube but instead wind around it), the resulting shape will be a superhelix whose pitch is believed to be given by the internal twist [12, 13]. Remarkably there is some evidence that, in contrast to the bacterial flagella filament and all other structures discussed, microtubules are super-helices that are spontaneously and permanently reshaping on experimental timescales: they change their reference ground state due to thermal fluctuations. This unusual collective movement was previously proposed and termed the “wobbling mode” [12, 13].

Notable phenomenological models for multistable helices have been developed in the past in order to describe transformations of bacterial flagella [17–19], coiled plant tendrils [20], or whole microorganisms [21, 22]. The novel and rather unique feature of our present model, that we will explore and illustrate here in depth, will be the extraordinary dynamic behavior associated with the cooperative “wobbling motion” of the filament. Although biofilaments are usually studied in the framework of beam elasticity, microtubules can also be modelled as cylindrically wrapped membranes since they are hollow. Jánosi *et al.*, for example, modelled microtubule walls as elastic sheets in order to analyze their elastic properties [23]. Inspired by the polymorphic tube model previously proposed by some of the authors [12, 13, 24] we study a tubular system that incorporates the idea of lattice confinement of bistable units and cooperativity into an elastic sheet. Numerical simulations and analytical models are combined here to provide an in-depth intuitive understanding of this system. The prestress, that will be built into our model, will give rise to a remarkable phenomenon: Localized conformational deformations, that will behave as quasiparticles, will emerge and govern the collective shape dynamics of the lattice via elastically-mediated interactions. When we switch on additional mechanical coupling terms in the lattice, these quasiparticles will exhibit cooperative interactions. The

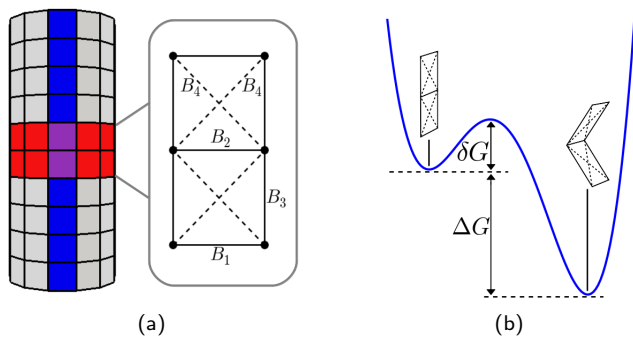


FIG. 1: (a) Construction of the polymorphic tube out of rectangular subunits (dimers). One ring of lateral neighbors is colored in red. One (proto-)filament formed by longitudinal neighbors is colored in blue. A rectangular subunit is divided into two squares by bonds  $B_2$ . Ghost diagonals  $B_4$  are added for shear rigidity. (b) Asymmetric double well potential for the bonds  $B_2$ .  $\Delta G$  denotes the energy difference between the straight and the curved state.  $\delta G$  is the height of the barrier with respect to the straight state.

cooperativity will lead to the formation of larger-scale “quasipolymer” superstructures that we will show to exhibit rather unusual collective dynamic modes. The notion of quasiparticles/-polymers is the most natural language to quantitatively describe many new phenomena for which we will collectively use the term “confotronic dynamics”.

In real biofilament systems this dynamics is usually inaccessible to direct observation. However, as the internal confotronic modes also govern the behavior of the centerline of the tube as a whole, their existence can be experimentally inferred from the observation of anomalous behaviors of the tube’s centerline in well chosen experiments. Among them, observing the dynamics of a tube clamped at one end, turns out to be the experiment of choice. We will see that a lot about the inner confotronic dynamics of quasiparticles can be revealed from the external behavior of the tube.

The paper starts with a description of the polymorphic tube model in Sec. II. In Sec. III, the notion of quasiparticles (called “confoplexes”) is presented in detail. We will see that these particles can form ordered conformational superstructures on the lattice (called “confostacks”). This order is shown to be responsible for the formation of the broken symmetry superhelical tube state, very much akin to the superhelices observed in microtubules and bacterial flagella. Finally, in Sec. IV the confotronic dynamics of clamped polymorphic tubes is analyzed with a particular focus on the remarkable collective mode (“wobbling mode”) that emerges spontaneously in the system at finite temperature.

## II. THE POLYMORPHIC TUBE MODEL

We construct a hollow polymorphic tube by discretizing its surface as a mesh of rectangular subunits (see Fig. 1(a)). Similarly to previous discrete models of (linear) elastic membranes [23, 25], the elastic properties of the tube will be enforced via stretching and bending energetic penalties of the mesh. The polymorphic character of the tube is implemented at the level of each subunit, decomposed into two squares, which is multistable and can be either straight or curved (see Fig. 1(b)). Note that this choice of mesh is well adapted to describe biofilaments such as microtubules. In this picture, each rectangular, double-square subunit of the mesh corresponds to a single tubulin dimer. The association of the former along the vertical direction defines protofilaments (blue in Fig. 1(a)) which form the tube in a way similar to protofilaments forming the wall of a microtubule. In this work we always consider 13 such protofilaments alluding again to microtubules. To stay as generic as possible, however, we will omit many system-specific details like the internal twist and other particularities of microtubules like the “seam” [23]. Such generic simplifications, including symmetry, are necessary in order to extract the physical “gist” of such systems, as we will see from the plethora of phenomena emerging already in this simplified lattice geometry.

Each dimer consists of internal and external bonds. The horizontal internal bond  $B_2$  separates the subunit into two squares and forms a *hinge* in the curved state of the dimer. The internal bonds  $B_4$ , depicted by dashed lines in Fig. 1(a), control the shearability of each square and ensure their planarity. The external bonds are shared with neighboring dimers: two bonds of type  $B_1$  along the vertical and four of type  $B_3$  along the horizontal direction. The elastic energy of the tube is a sum of contributions for stretching and bending of the mesh,  $E = E^S + E^B$ . Denoting  $\mathbf{d}_i$  the vector associated to a bond of type  $B_i$ , the total stretching energy of *all* bonds of type  $B_i$  is given by

$$E_i^S = \frac{1}{2} \mu_{si} \sum_{\{\mathbf{d}_i\}} \left( |\mathbf{d}_i| - d_i^{(0)} \right)^2, \quad i = 1, 2, 3, 4 \quad (1)$$

in the harmonic approximation. The sum runs over all the edge vectors  $\mathbf{d}_i$  of the tube. In Eq. (1),  $d_i^{(0)}$  is the preferred length of the bond  $B_i$  when the tube is in its straight cylindrical state (Fig. 1(a)) and  $\mu_{si}$  is the stretching rigidity. The stretching energy of the whole mesh is thus:  $E^S = \sum_{i=1}^4 E_i^S$ .

Similarly, we associate a quadratic bending energy with all bonds of type  $B_1, B_3, B_4$ :

$$E_i^{BH} = \frac{1}{2} \mu_{bi} \sum_{\{s_i\}} \left( s_i - s_i^{(0)} \right)^2, \quad i = 1, 3, 4 \quad (2)$$

where  $s_i = (\mathbf{n}^a \times \mathbf{n}^b) \cdot \frac{\mathbf{d}_i}{|\mathbf{d}_i|}$  is the sine of the angle between the outward normals  $\mathbf{n}$  of two adjacent triangles  $a$  and  $b$

at bond  $\mathbf{d}_i$ , and  $\mu_{bi}$  is the bending rigidity of this bond. The constants  $s_i^{(0)}$  are chosen such to enforce the straight cylindrical state. To allow the subunits to accommodate two stable conformations, we assign an anharmonic bending potential  $E_2^{\text{BAH}}$  for all bonds of type  $B_2$ :

$$E_2^{\text{BAH}} = \sum_{\{s_2\}} (As_2^4 + Bs_2^3 + Cs_2^2), \quad (3)$$

where the coefficients  $A$ ,  $B$ , and  $C$  are all functions of the energy difference  $\Delta G$  and the barrier  $\delta G$  and are chosen to favor the curved state (see Fig. 1(b)). The total bending energy of the mesh is thus  $E^{\text{B}} = E_1^{\text{BH}} + E_2^{\text{BAH}} + E_3^{\text{BH}} + E_4^{\text{BH}}$ .

In the following, the values of the stretching rigidities will be expressed in units of  $k_B T_0/d^2$  and the bending rigidities in units of  $k_B T_0$ , where  $T_0$  is the room temperature and  $d = 4$  nm the size of a monomer (see appendix A for all the parameter values). The temperature  $T$  in the simulations will be measured in units of  $T_0$ .

### III. CONFOPLEXES, CONFOSTACKS AND SPONTANEOUS SYMMETRY BREAKING

The rich conformational properties of the previously defined tube model will now be analyzed with the help of numerical simulations and phenomenological models. The large number of parameters of the model is a serious limitation for exploring all possible conformations in an attempt to build a complete phase diagram. Instead, we reduce the number of independent parameters as much as possible and look for interesting generic configurations and behavior. In this spirit, we set  $\mu_s = \mu_{s1} = \mu_{s2} = \mu_{s3}$  and choose their value in the typical range of the elastic constants of microtubules [23] (see below). To facilitate the visual and numerical detection of the characteristic behavior for the short lattices practically accessible to our simulations, we have deliberately chosen an intrinsic curvature of the protofilaments much larger than for real microtubules. The other parameters are adjusted to ensure the numerical stability of the mesh (see appendix A).

We first discuss the results of the numerical simulations in which the system is integrated in time with the Langevin Dynamics method (see again appendix A). To understand the subtle competition between the anharmonic potential (3) and the elasticity of the lattice, our study is built up in a hierarchical manner: first the different conformations of a single section of a tube are explored, from which, in a second step, we can understand the behavior of longer tubes. Finally, long tubes with additional cooperative interactions along the protofilaments are studied.

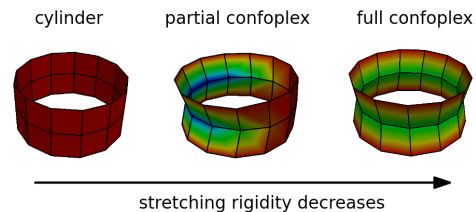


FIG. 2: Three configurations for one ring of dimers depending on the stretching rigidity  $\mu_s$ : the straight cylinder, a partial confoplex, and a full confoplex for which all dimers are in the curved state.

#### A. Numerical simulations

##### 1. A single section of the tube, the emergence of a confoplex

We first consider the ground state (zero temperature limit) of a single section of the tube. By varying the elastic stretching constant  $\mu_s$  we observe three different types of configurations (see Fig. 2): For sufficiently large values of  $\mu_s$  (at the order of  $10^5$ ) the dimers can not switch to their curved configuration and the ring maintains its cylindrical form. However, when  $\mu_s$  becomes smaller ( $2 \times 10^4$ ), all subunits adopt a curved conformation, forming what we call a “conformational complex” or—more briefly—a *confoplex*. The ring is still cylindrically symmetric but its shape is catenoid-like. Very interestingly, for intermediate values of  $\mu_s$  (around  $4 \times 10^4$ ) a state with *broken cylindrical symmetry* is the minimum-energy configuration. In this *partial confoplex* conformation a cluster of neighboring dimers on one side of the ring is switched to the curved state, thereby creating a negatively curved scar which gradually decays towards the opposite side of the tube. This causes the opposite wall to bulge slightly outwards.

##### 2. Interacting confoplexes

The emergence of full and partial confoplexes in the ring leads to the interesting question of how single confoplexes interact with each other in a larger lattice. In contrast to the single section, which does not possess any longitudinal neighbors, the bending around the bonds of type  $B_1$  will now have an important effect. For the case of full confoplexes successive sections meet at positive curvatures at the  $B_1$  bonds. Hence, for non-zero  $\mu_{b1}$ , stacking one full confoplex on top of a second one will cost some energy; when the value of  $\mu_{b1}$  is high enough to dominate the other terms, the tube goes back to the straight configuration.

For values of  $\mu_s$  for which the tube is composed of partial confoplexes, the deflection of each section is expected to be in almost independent directions if  $\mu_{b1}$  is zero. (In fact, they are not completely uncorrelated due to the stretching energy of the bonds  $B_1$ .) This almost random

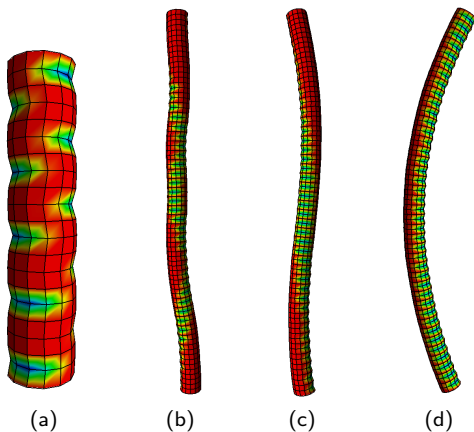


FIG. 3: (a) Repulsive partial confoplexes form a zigzag pattern on the tube ( $\mu_{b1} = 300$ ,  $T = 3$ ). (b)–(d) Simulation snapshots for a system with fixed cooperativity  $\mu_c = 50$  and  $N = 40$  segments at a temperature  $T = 3$ . (b) The repulsive interactions are dominant for large  $\mu_{b1} = 300$ . (c) For weaker repulsion ( $\mu_{b1} = 200$ ) a large-scale order emerges. (d) For  $\mu_{b1} = 0$ , the tube deflects into a C-like shape.

mutual orientation has been confirmed by simulations at finite temperature (not shown). However, for non-zero values of  $\mu_{b1}$ , (e.g. for  $\mu_{b1} = 300$ ), each section conserves its partial confoplex configuration but neighboring confoplexes tend to align their orientation opposite to each other, forming an “antiferromagnetic”-like zigzag pattern along the tube (see Fig. 3(a) for an example at temperature  $T=3$ ). If we keep increasing  $\mu_{b1}$ , the confoplexes become gradually smaller in size and finally vanish, similar to the catenoid-to-cylinder transition found for the ring when  $\mu_s$  is increasing.

### 3. Cooperativity: confostacks, helices and spontaneous symmetry breaking

The repulsive interaction of confoplexes implies that global conformational superstructures of the tube are formed only if neighboring confoplexes interact cooperatively via additional interactions. Cooperative interactions among monomers in a filament have been observed, for example, in single protofilaments of microtubules *in vitro* [15]. Motivated by this observation, we implement the coupling between neighboring dimers on a protofilament by adding a cooperative interaction between the angles associated to the anharmonic bonds  $B_2$ :

$$E^{\text{CP}} = \frac{\mu_c}{2} \sum_{\{s_2\}} \left( (s_2 - s_{2,\text{next}})^2 + (s_2 - s_{2,\text{prev}})^2 \right), \quad (4)$$

where  $\mu_c$  is the strength of the cooperative interaction between a bond  $B_2$  and its nearest neighbors (i.e.,  $B_2$ -next and  $B_2$ -previous). In the presence of partial confoplexes this term causes an attractive interaction between them, opposing the repulsive one (due to the bending  $\mu_{b1}$ ) and

generating an interesting “frustrated” situation. The attraction between neighboring partial confoplexes leads to a stack of confoplexes forming a kind of “quasipolymer” superstructure arrangement on the lattice. This particular internal state of the lattice, being an ordered stack of confoplexes, will from now on be called a “*confostack*”. In a similar manner as the emergence of the confoplex previously gave rise to the breaking of the cylindrical symmetry on the *single section scale*, the formation of the ordered confostack is responsible for the spontaneous breaking of the *large scale* chiral symmetry of the tube centerline in the three-dimensional space.

At finite temperature, thermal fluctuations tend to disorganize the ordered confostack. In this case we observe the formation of uncorrelated fluctuating domains of ordered confoplexes distributed along the confostack. The characteristic size of such a domain will be called the coherence length of the confostack and denoted with  $l_c$ . This coherence length shares some analogy to the concept of persistence length of a semiflexible polymer. In particular we can write  $l_c = C/(k_B T)$  where  $C$  (an unknown function of the material parameters) can be seen as an effective stiffness of the confostack. Note that an exact computation of  $l_c$  for a simplified model of microtubules can be found in Ref. [24]. We expect two extreme situations: For a tube of length  $L$  such that  $L \ll l_c$ , the confostack is fully ordered and the entire tube breaks the cylindrical symmetry. For  $L \gg l_c$ , the confostack is made up of a juxtaposition of uncorrelated fluctuating domains of ordered confoplexes leading to a statistically straight tube on average.

What is the fundamental shape of a single domain of an ordered stack of confoplexes? The answer comes from the numerical simulations. Figs. 3(b)-3(d) show a number of snapshots of the typical configurations of the tube at finite temperature for increasing values of the ratio  $\nu := \mu_c/\mu_{b1}$ . In Fig. 3(b) where  $\nu$  is small, we see that the confostack is made of short coherent helices of random handedness. This corresponds to the situation  $L \gg l_c$ , where the tube looks straight on long scales, since right- and left-handed helices cancel each other out. The fundamental shape of a domain of ordered confoplexes is thus a helix with a pitch which depends on  $\nu$ . The origin of this helicity will be elucidated below in section III B 2.

Increasing  $\nu$  leads to a stronger alignment of the partial confoplexes, i.e., an increase of the pitch of the confostack. When the coherence length is larger than  $L$  but the pitch is still smaller than  $L$ , the switched dimers form a coherent helical confostack, deflecting the centerline of the tube into a superhelix in space as shown in Fig. 3(c). Note that the superhelices of either handedness appear spontaneously within a completely symmetric lattice. This can be seen as an indication that real microtubules might form superhelices with finite pitches by a similar spontaneous symmetry breaking mechanism, even in the absence of an explicit internal lattice twist [12, 13]. For very large  $\nu$  the cooperativity is strong enough for the pitch of the helical confostack to become larger than

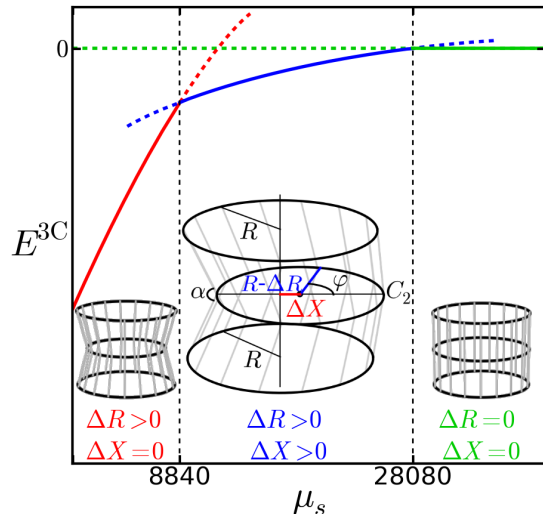


FIG. 4: Elastic energy of a lattice section as a function of the stretching rigidity  $\mu_s$  in the simple model.

*L.* Fig. 3(d) shows such a situation with  $L \ll l_c$ . In this case the tube forms a circular arc with an untwisted confostack living on it.

## B. Phenomenological modelling

After outlining the empirical observations of various interesting phenomena from the Langevin simulations in the previous section, in this section we seek to analytically and phenomenologically explain the observations. In the first subsection we will explore how the very existence of full/partial confoplexes can be qualitatively understood within a simple analytical model. Following that, in the second subsection, we outline a simple phenomenological model explaining the chiral symmetry breaking and the formation of the left-/right-handed superhelical confostacks.

### 1. Simple model for confoplex formation

In this section we revisit the transitions between the different states of a single section (cylinder, partial and full confoplex) and will explain them qualitatively. For all three states in Fig. 2, we observe that the horizontal bonds form polygons which are close to circles lying in three parallel planes. For a full catenoid-like confoplex, we see that the circle in the middle (called  $C_2$  because it is associated to the anharmonic bonds  $B_2$ ) has the smallest radius, whereas for the partial confoplex there is additionally a small shift of the center of  $C_2$ . This shift is in the direction of the non-switched region of the wall, which thus bulges slightly outwards. In view of these observations, it is tempting to approximate a section of the tube by three circles that will interact elastically in

a very simplified manner (thus the results can only be qualitatively compared with the simulation). By fixing the center position and the radius  $R$  of the lower and upper circles, the only variables are now the position and the radius of the circle  $C_2$  in the middle. This circle can shift its center horizontally by an amount of  $\Delta X$ . It can also decrease its radius  $R$  by  $\Delta R$  with an energy cost

$$E_s = \frac{\mu_s}{26} (2\pi\Delta R)^2, \quad (5)$$

where  $\mu_s$  is the stretching rigidity of  $C_2$ . For a confoplex there is an additional cost of bending energy due to the angle  $\alpha$  between the lines joining the three circles at an azimuthal position  $\varphi$  of  $C_2$  (see Fig. 4). This angle is chosen negative in the concave part of the confoplex and given by  $\sin \alpha \approx -2(\Delta R - \Delta X \cos(\varphi))$  to first order in  $\Delta R$  and  $\Delta X$ . Similar to the anharmonic bending energy (3) for the bonds  $B_2$  used in the simulations, we write the bending energy of the simple model as a double well potential and integrate it along  $C_2$ :

$$E_b = \oint_{C_2} (A(\sin \alpha)^4 + B(\sin \alpha)^3 + C(\sin \alpha)^2) d\varphi. \quad (6)$$

By minimizing the total energy of this three circle model,  $E^{3C} = E_s + E_b$ , with respect to  $\Delta X$  and  $\Delta R$ , we observe the same three configurations as in the numerical simulations (see Fig. 4 again): for increasing  $\mu_s$  the ground state shifts from a full confoplex ( $\Delta R > 0$ ,  $\Delta X = 0$ ) where  $C_2$  can easily stretch, to a partial one ( $\Delta R > 0$  and  $\Delta X > 0$ ) which is the result of a compromise between the stretching and the anharmonic bending energy. For an even larger stretching constant we finally obtain a cylinder ( $\Delta R = \Delta X = 0$ ). This simplified model which only comprises the stretching energy and the anharmonic bending potential of the bond  $B_2$  gives a simple explanation for the very existence of confoplexes. Of course, this reduced model is not capable to predict the precise transition values; nonetheless it provides a qualitative explanation for the observed morphologies in the simulation. Due to its simplicity, it is highly intuitive and also analytically tractable.

### 2. Elastically-mediated interactions between confoplexes and formation of confostacks

From what we learnt previously from the simulations, the shape of the confostack results from the competition between the cooperative attractive interaction and the elastic repulsion between partial confoplexes (see Fig. 3). If both interactions were short-ranged, one would observe the two configurations depicted in Fig. 5(a) with equal probability as they would have equal energies.

But the observed spontaneous symmetry breaking of the straight tube, which leads to right- and left-handed superhelices, can only be explained by the presence of an effective *long-range* repulsion between the confoplexes. Intuitively, the confoplexes can be seen as quasiparticles

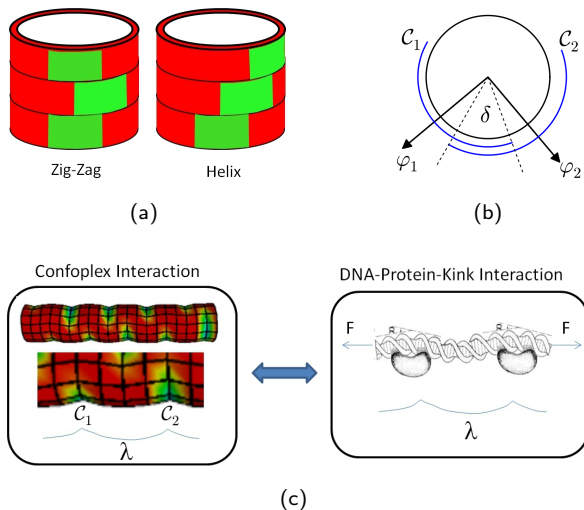


FIG. 5: (a) Possible quasiparticle conformations for a short tube if the cooperative attractive interaction and the elastic repulsion between neighboring partial confoplexes is included into the model. (b) Variables used for measuring the overlap of two confoplexes  $C_1$  and  $C_2$ . (c) Analogy between interacting confoplexes and proteins bound to a semiflexible filament (picture adapted from [26], reprinted with permission from Elsevier), see text.

which deform the lattice surrounding them, generating an extended elastic field. As a consequence the confoplexes will interact with each other through long-range elastically-mediated repulsive forces, extending further away than to the nearest neighbors.

A full analytical treatment of this interaction in our concrete case is complicated by the presence of various lattice parameters in the simulation, but a qualitative understanding is possible if we retain only the dominant contributions. In this spirit, consider two confoplexes  $C_1$  and  $C_2$  which azimuthally overlap with an angle  $\delta$  (cf. Fig. 5(b)) and interact only elastically without cooperativity (left image of Fig. 5(c)). For simplicity, let us assume that only the overlapping parts of  $C_1$  and  $C_2$  interact strongly with each other. This seems reasonable, since the elastic interaction between the parts of the confoplexes which do not sit on the same protofilament will be more screened around the tube. If the confoplexes are shifted by an angle  $\Delta\varphi = |\varphi_1 - \varphi_2|$  their interaction is then proportional to the overlap angle  $\delta$ , and we can write

$$E_{C_1-C_2} \approx \frac{13\delta}{2\pi} E_{C-C}^{\text{single PF}}, \quad (7)$$

where  $E_{C-C}^{\text{single PF}}$  is the interaction energy of the parts of the two partial confoplexes sitting on the same protofilament. For a small angular deviation  $\theta(u)$  with respect to the straight protofilament state this energy can be ap-

proximated as

$$E_{C-C}^{\text{single PF}} = \frac{1}{2} \int_0^L \left( B_{\text{eff}} \left( \frac{d\theta}{du} \right)^2 + F_{\text{eff}} \theta^2 \right) du, \quad (8)$$

where  $u$  is the arc length along the protofilament,  $B_{\text{eff}} \approx \mu_{b1}d$  is the bending rigidity of the protofilament and  $F_{\text{eff}} \approx \mu_s d$  is an intrinsic effective tension due to the stretching rigidity of the bonds of the protofilament.

Eq. (8) is formally equivalent to the interaction energy of two proteins bound to the same side of a semiflexible filament under an external pulling force. As shown in [26] the elastic interaction is repulsive. Similarly, cylindrical proteins bound to a locally flat membrane are described with the same energy functional and repel as well [27–30]). The range of this repulsion is given by an elastic screening length  $\lambda = \sqrt{B_{\text{eff}}/F_{\text{eff}}}$  (see Fig. 5(c)).

Despite the crude approximations considered here the basic physics of the interaction is well captured. In the presence of cooperativity, this long-range interaction leads to an interplay between nearest and next-nearest neighbor repulsion between the quasiparticles; at short scale the second configuration in Fig. 5(a) will be adopted. At a larger scale the quasipolymer will thus form a helix on the lattice inducing a superhelical structure of the tube in three-dimensional space.

Before embarking on the study of the dynamic properties of polymorphic tubes, it is interesting to remark, that the notion of quasiparticles, interacting by elastic fields in our present case is rather similar to the notion of “twist-kinks”, the quasiparticles formed in squeezed helices confined to two dimensions [9]. In this context conformational “twist-kink” quasiparticles appear as a natural concept as well, indicating a broader relevance of this perspective for prestressed filaments with (hidden) internal degrees of freedom.

#### IV. DYNAMICS OF CLAMPED TUBES: CONFOSTACKS DIFFUSE THROUGH THE LATTICE

The observation of microtubules clamped at one end has been a key experiment revealing their anomalous behavior [31, 32] and was the starting point for the polymorphic tube model proposed in [12, 13]. In this section we explore the dynamics of collective internal modes of the lattice by simulating a tube of various lengths clamped at one end, at finite temperature  $T$ . We focus on the simplest case in which the tubes form circular arcs (helices with infinite pitch), *i.e.*, when they bear ideal untwisted confostacks with a coherence length much larger than the tube’s length.

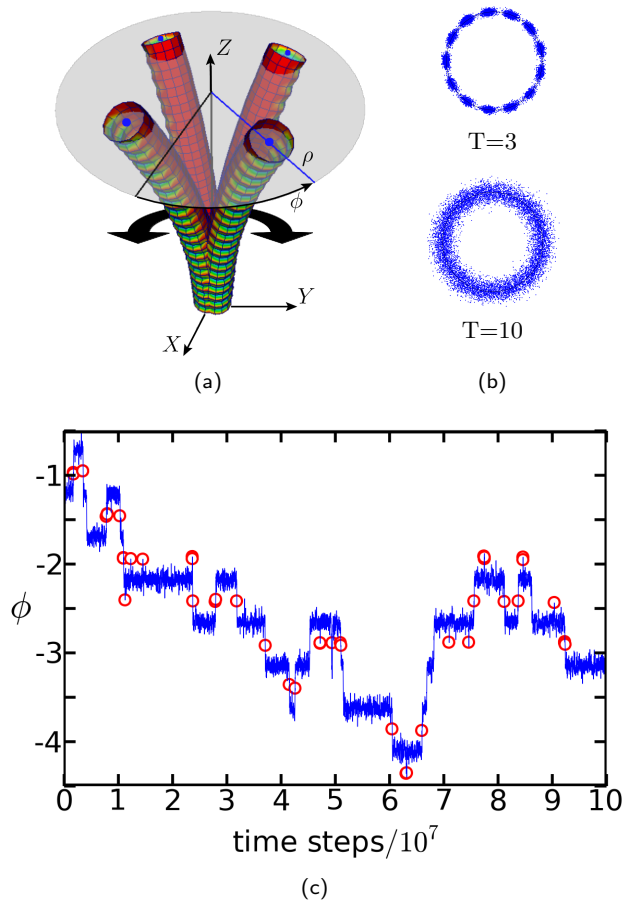


FIG. 6: (a) Rotating confostack clamped at the bottom end at finite temperature  $T$ . The arc-shaped tube diffuses randomly around a fixed axis. (b) Diffusion of the end point of the tube’s centerline for  $T = 3$  and  $T = 10$ . For low temperatures the periodic energy barrier  $V(\phi)$  becomes apparent in the diffusion pattern. (c) Temporal evolution of the azimuthal angle  $\phi$  of the end point of the tube’s centerline at  $T = 3$ . The red circles highlight the transition regions in which the confostack is at the maximum of the barrier (within  $\pm 0.05$  radian from the location of this maximum).

## A. Numerical simulations

### 1. Observation of the wobbling motion

Even though the rigid attachment of the arc-shaped tube seems to preclude large scale motion, the tube is not static in shape. Instead, we clearly observe a random rotation of the tube around a fixed axis (see Fig. 6(a)) in agreement with the predictions of the wobbling motion for polymorphic tubes [12, 13]. It is intuitively clear that the symmetry-broken circular arc state can in principle explore all its equivalent sister states, with the arc pointing in one of 13 possible directions. However, it seems not obvious a priori if the switching between the states can practically occur, and if so, on which timescale. To

quantify the dynamic behavior of this collective “wobbling mode”, we measure the time evolution of the centerline at the free end, which diffuses inside an annular strip in the  $\rho\phi$  plane (see Fig. 6(b)).

If the clamped tube was not polymorphic, but had the shape of a *static* circular arc instead, its elastic fluctuations could be simply decomposed into a radial and an azimuthal elastic mode. In this case we would expect a classical “wormlike chain” dynamic behavior, where the chain has merely an intrinsic curvature. However, such an intrinsically curved elastic filament would of course not rotate. In sharp contrast to the wormlike chain case, the observed wobbling scenario allows an efficient rotation (despite the fixed clamping of the end section) in our system. This rotary motion, which is the very signature of a polymorphic lattice with broken symmetry, is apparently caused by a confostack that moves azimuthally around the lattice.

Note that we have a peculiarly interesting “polymer on a polymer” motif here: A quasipolymeric entity (the confostack) exists and moves on the surface of a tube, that itself can be considered as a polymer on larger scales. The experimentally observable motion of the tube is slaved to the motion of the confostack. The latter might be practically hidden from direct experimental detection but it affects the tube’s centerline dynamics so severely that it becomes detectable by tracing the tube’s centerline.

### 2. Energy barrier

A closer look at the distribution of the azimuthal angle  $\phi$  of the tube’s end reveals that the distribution is centered around discrete angular values  $\frac{2\pi n}{13}$ ,  $n \in \mathbb{Z}$ , corresponding to the 13 protofilaments (c.f. the blobs in Fig. 6(b)). This result unveils the existence of a periodic potential  $V(\phi)$ —due to the discrete lattice structure—in which both the confostack and in turn also the free end of the tube diffuses. Although the azimuthal rotation of the confostack can in principle be continuous, it tends to visit the minimum of  $V(\phi)$  much more frequently. This potential is associated with an effective energy barrier  $\Delta E$  over which the confostack has to hop in order to move azimuthally on the lattice from one minimum of  $V(\phi)$  to the next one. The consequences of  $\Delta E$  on the confostack movement will be revisited and explored later on. Fig. 7 shows a histogram of the logarithm of the angular distribution function of the end of the centerline which equals  $-V(\phi)/(k_B T)$  modulo  $\frac{2\pi}{13}$ . This yields a first estimate of the barrier  $\Delta E$  measured from the difference between the maximum and the minimum of  $V(\phi)$ :  $\Delta E \approx 12.5$ . As we will see in Secs. IV B 2 and IV B 3, the same value will be found with two other methods and is independent of the length  $L$  of the tube for all the lengths considered in the simulations.

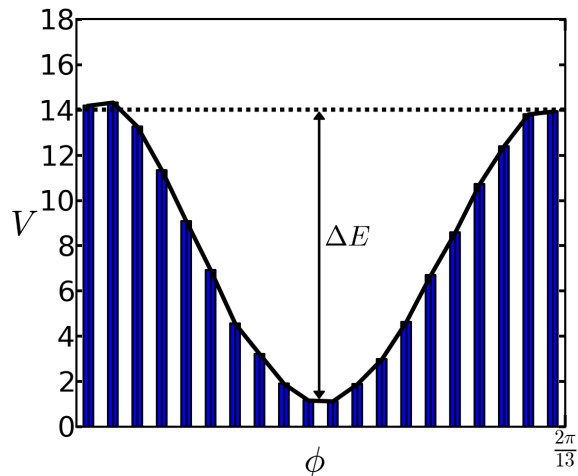


FIG. 7: Histogram of the structural barrier  $V(\phi)$  obtained from the angular distribution function at  $T = 3$  and  $N = 20$ .

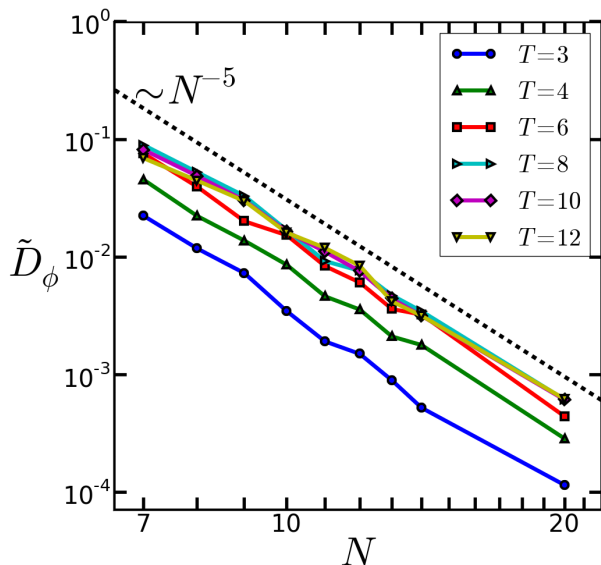


FIG. 8: Measured scaled diffusion coefficient (the mobility) of the wobbling mode  $\tilde{D}_\phi = D_\phi / (k_B T)$  as a function of the number of sections  $N$  of the tube for different temperatures  $T$ .

### 3. Rotary diffusion of the clamped tube

From the simulations one can get a more quantitative understanding of the wobbling mode kinetics by measuring the mean square displacement of the azimuthal angle  $\phi$  of the end point of the centerline of the tube. These measurements have been performed for tubes of various lengths  $L = 2Nd$  (with  $N$  the number of sections of the tube) and at different temperatures  $T$ . The results display the typical behavior of a diffusive system with a diffusion coefficient  $D_\phi$ :  $\langle (\phi(t+t_0) - \phi(t_0))^2 \rangle = 2D_\phi t$ . In

Fig. 8 we observe that the diffusion coefficients normalized by the corresponding temperatures (the mobility)  $\tilde{D}_\phi = D_\phi / (k_B T)$  all scale with the length as  $N^{-5}$  but do not collapse to a single temperature-independent curve.

The scaling of the diffusion constant with length  $\tilde{D}_\phi \sim N^{-5}$  is typical for a rotating rigid circular arc moving through a fluid. The normalized diffusion coefficient in this case is given by (see Appendix B)  $\tilde{D}_{\phi_0} = \frac{5}{8} \frac{N^{-5}}{\xi_\perp \kappa^2 d^5}$ , where  $\kappa$  is the curvature of the arc and  $\xi_\perp$  the friction constant per unit length.

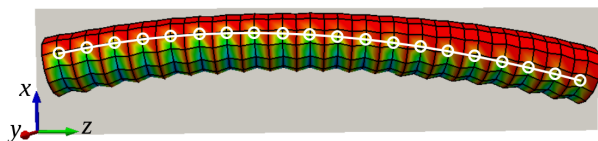
The temperature dependence of  $\tilde{D}_\phi$  is much more intriguing. Naïvely, we would expect that, like for a rigid rotor moving through a fluid,  $\tilde{D}_\phi$  is simply a constant with respect to the temperature. However, this expectation is too simple as it considers only the friction of the rotating arc through the external fluid medium and misses the internal dynamics of the confostack, in particular the presence of structural barriers, as discussed in the previous section. This hidden internal dynamics nevertheless reflects itself in the movement of the end point of the tube and leads to an additional internal dissipation.

In summary, the simulations reveal that the tube's friction must result from a combination of the external friction of the arc in the fluid medium and a yet to be characterized internal dissipation mechanism. In the next section, we explore the origin of this inner dissipation mechanism. In particular, we take a closer look at the conformational mode responsible for these inner losses via barrier crossing.

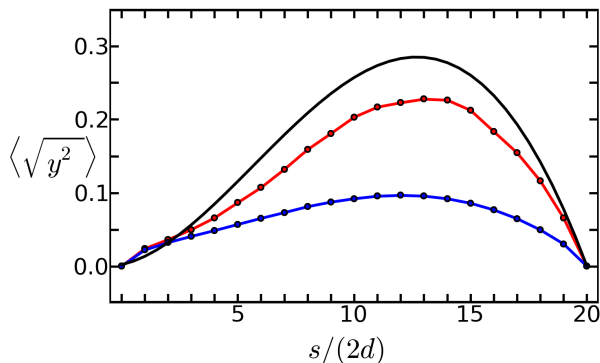
### 4. Barrier crossing transition state: The confostack-kink

Until now, we have analyzed the wobbling motion by tracking the time evolution of the end point of the centerline. In this section we go a step further and take advantage of the simulation to directly observe the shape of the confostack on the surface of the lattice. At zero temperature, the tube assumes one of its circular ground states oriented along one of the 13 possible orientations. At any finite temperature, thermal excitations allow for a continuous shape reorientation of the confostack between the ground states by crossing the energy barrier  $\Delta E$ , while at the same time reorienting the direction of the tube's curvature.

What is the critical confostack mode, *i.e.*, the conformation of the confostack at the top of the energy barrier  $\Delta E$ ? A naïve first look into the noisy simulation snapshots of the tube in space does not allow to identify the critical conformational mode on the barrier (at the transition) in a simple way. But if one rotates the tube in its natural co-moving frame of reference first (see next section for details), one can observe the behavior of the confostack on the surface of the tube in detail. This frame is defined by the  $xz$  plane formed by the attachment point and the end of the centerline of the tube. Therefore, the deflection perpendicular to the  $xz$  plane,  $y(s)$ , satisfies



(a)



(b)

FIG. 9: (a) Simulation snapshot of a tube ( $T = 3$ ,  $N = 20$ ) in the transition state regime. The tube is rotated into its natural comoving frame in which the two ends of the tube’s centerline lie in the same plane  $xz$ . The shape of the confostack resembles a kink which interpolates between two neighboring protofilaments. This is the typical configurational mode of the transition for large  $N$ . (b) Root mean square of the deflection  $y(s)$  of all states (blue), the transition states (red), and the theoretical prediction for the transition states (black).

the condition  $y(0) = y(L)$ , where  $s$  is the arc length of the centerline. At zero temperature, the confostack lies in the  $xz$  plane and the centerline of the tube is a circular arc. In this case the co-moving and the laboratory frames are identical. At finite temperature and for the transition regions, we typically observe a confostack forming a kink on the lattice which will propagate until the whole structure has crossed the barrier (see Fig. 9(a) for a snapshot). This confostack-kink resembles a “polymorphic” dislocation that can be either left- or right-handed, while reorienting the direction of the whole tube.

To capture and characterize the shape of the confostack-kink under the conditions of strong thermal noise, we have looked for statistical anomalies of the tube’s shape in the co-moving coordinates. Since the centerline of the tube leaves the  $xz$  plane only slightly, we expect that  $x(s)$  still describes a circular arc approximately ( $x(s) \approx \frac{1}{2}\kappa s^2$ ). This is confirmed by the numerical data (not shown). What turns out to be more interesting is the  $y$  direction. The root mean square  $\langle \sqrt{y^2(s)} \rangle_{\text{Tr}}$  of the deflection  $y(s)$  of the centerline is computed over all transition states (red circles in Fig. 6(c)). They correspond to the critical confostack-kink at the top of the energy barrier  $\Delta E$ . This kink can either move to the next minimum of the periodic potential  $V(\phi)$  or return to the original minimum. The curve  $\langle \sqrt{y^2(s)} \rangle_{\text{Tr}}$  is significantly different from the

measurement of the same quantity for all—transition and non-transition—states of the simulation taken together  $\langle \sqrt{y^2(s)} \rangle_{\text{All}}$  as shown in Fig. 9(b).

## B. Theory of the dynamics of the clamped tube

To understand the unusual dynamics of the clamped tube observed in the simulations and to interpret the behavior of the confostack-kink at the barrier, in this section we make some theoretical developments.

### 1. Modelling a single confostack-kink

We first define an external laboratory frame  $(X, Y, Z)$ . The tube is clamped at the origin and is oriented in the  $Z$  direction. For small deviations around the  $Z$  axis, the unit vector tangent to the tube’s centerline is approximately given by  $\mathbf{t} \approx (\theta_X, \theta_Y, 1)$  with  $\theta_{X/Y}$  the deflection angles of the centerline in the  $X/Y$  direction. This deflection can be decomposed as the sum  $\theta_{X/Y} = \theta_{\text{el},X/Y} + \theta_{\text{pol},X/Y}$  of a purely elastic deviation and a polymorphic one [13]. The polymorphic contribution can be expressed in terms of a polymorphic phase  $\varphi(s)$  which stands for the confostack’s angular orientation with respect to the tube’s material frame. Therefore, one has  $\theta_{\text{pol},X}(s) = \kappa \int_0^s \cos \varphi(s') ds'$  and  $\theta_{\text{pol},Y}(s) = \kappa \int_0^s \sin \varphi(s') ds'$ . Neglecting the purely elastic fluctuations, the lateral displacement of the tube in the  $(X, Y)$  plane can be written as

$$\begin{aligned} X(s) &= \int_0^s \sin [\theta_{\text{pol},X}(s')] ds', \quad \text{and} \\ Y(s) &= \int_0^s \sin [\theta_{\text{pol},Y}(s')] ds'. \end{aligned} \quad (9)$$

As defined previously, the co-moving frame  $(x, y, z = Z)$  is given by the rotation

$$\begin{aligned} x(s) &= X(s) \cos \Phi + Y(s) \sin \Phi, \\ y(s) &= -X(s) \sin \Phi + Y(s) \cos \Phi \end{aligned} \quad (10)$$

with  $\Phi = \arctan(Y(L)/X(L))$ . Once we know the polymorphic phase  $\varphi(s)$  of the confostack configuration in the transition regime we can determine the deflections  $(x(s), y(s))$  of the centerline in the co-moving frame with the help of Eqs. (10) and compare them with the experimental data. To model the behavior of the confostack phenomenologically, we assume that it moves along a tube of length  $L = 2Nd$  in a periodic potential of amplitude  $W$  with an effective polymorphic stiffness  $C_p$ :

$$\Delta E(L) = \int_{-L/2}^{L/2} ds \left\{ \frac{C_p}{2} \varphi'^2 + \frac{W}{2} [1 + \cos(13\varphi)] \right\}, \quad (11)$$

where the interval of the arc length  $s$  of the centerline has been shifted for mathematical convenience  $s \in$

$[-L/2, L/2]$ . The transition state is found by minimizing  $\Delta E(L)$  with the natural boundary conditions  $\varphi'(\pm L/2) = 0$ , *i.e.*, no torque at the confostack ends. As shown in Appendix C there are two regimes:

a) For  $L < \pi\ell$  with  $\ell = \sqrt{2C_p/(13^2W)}$ , the minimal energy barrier-crossing configuration is  $\varphi(s) = 0$ . This corresponds to a uniform rotation of the confostack as a block over the barrier. In this case the barrier energy grows linearly with the length,  $\Delta E(L) = WL$ .

b) For  $L > \pi\ell$ , a nontrivial barrier crossing solution minimizing  $\Delta E(L)$  is:

$$\varphi(s) = \frac{2}{13} \arcsin \left( \frac{1}{\sqrt{m}} \operatorname{sn} \left[ \frac{s}{\ell}, 1/m \right] \right), \quad (12)$$

where  $\operatorname{sn}$  is the Jacobi sine function of parameter  $m > 1$  [33]. Eqn. (12) is a periodic function in  $s$ . The solution which is monotonous and interpolates between two successive minima of the periodic potential lies on a finite interval given by the condition  $L(m) = 2\ell K[1/m]$ , where  $K[1/m]$  is the complete elliptic integral of the first kind. In the limit of large tube lengths  $L$ , we have  $m \approx 1$  and the transition state confostack Eq. (12) becomes a kink:

$$\varphi(s) = (4 \arctan(e^{\frac{s-s_0}{\ell}}) - \pi)/13 \quad (13)$$

where  $s_0$  is the position of the center of the kink on the lattice.

To determine the typical size of the confostack at the transition, we look at the energy of the solution (12) computed in Appendix C (see Eq. (C5)). In the regime where the length  $L \geq \pi\ell$ , the barrier  $\Delta E(L)$  grows sublinearly and saturates at  $\Delta E \approx 0.05C_p/\ell$  for large  $L$ . As already mentioned, the notable observation from the computer simulation is that  $\Delta E \approx 12.5$  for all the lengths considered in the simulations,  $L \geq 14d$ . Therefore,  $\ell \ll L$  and Eq. (13) is a good approximation for the typical confostack configuration at the transition. This analysis of a single confostack-kink allows us to determine the theoretical root mean square of  $y(s)$  at the transition which can then be compared to the simulations.

## 2. Deflection of the tube at the transition

Assume that there is only a single confostack-kink of very short size  $\ell \approx 0$  placed on a random segment ( $n = 1, 2, \dots, N$ ) of the tube. Averaging over all positions of the kink with the same probability we have computed  $\langle \sqrt{y^2(s)} \rangle_{\text{model}}$  numerically for  $N = 20$  as shown in Fig. 9(b). We find that the model is close to the simulation data of the transition state. This agreement is reassuring and validates the idea of the confostack-kink as the main culprit for the crossing of the angular barrier. In addition, from the ratio of  $\langle \sqrt{y^2(s)} \rangle$  in this model over the simulation data for all frames (transition and non-transition states) we can infer the kink density in

the simulation. Indeed the probability to find the kink anywhere is  $P \approx \frac{\max(\langle \sqrt{y^2(s)} \rangle_{\text{All}})}{\max(\langle \sqrt{y^2(s)} \rangle_{\text{model}})} \approx 0.368$ . Therefore,

the kinks are roughly three times more frequent in the transition states as expected from a kink-mediated barrier crossing mechanism.

This result allows us to determine  $\Delta E$  in another way: The probability of finding a single kink on any segment of the tube ( $n = 1, 2, \dots, N$ ) is given by:

$$P_1 = \frac{\exp(-\frac{\Delta E}{k_B T})}{1 + \exp(-\frac{\Delta E}{k_B T})}. \quad (14)$$

The probability to find at least one kink on the tube is then given by  $P = 1 - (1 - P_1)^N$ . For a tube with  $N = 20$  segments at  $T = 3$  we find that  $P \approx 0.368$  leads to an energy barrier  $\Delta E \approx 12.5$  in agreement with the simulations. The corresponding  $P_1 \approx 0.018$  shows that for  $N = 20$  the density of kinks is  $NP_1 \approx 0.37$ . Since the kinks are roughly three times more frequent at the transition we deduce that the density of kinks at the transition is about one which justifies our original assumption.

## 3. Rotor diffusion revisited

The theoretical modelling in the previous sections allowed us to deepen our understanding of the confostack dynamics in the presence of a barrier. With this knowledge we can return to the anomalous diffusion of the clamped tube. Approximating the internal periodic barrier  $V(\phi)$  by a sinusoidal of the form  $V(\phi) = (\Delta E/2) \cos(13\phi)$ , the azimuthal diffusion coefficient  $D_\phi$  of the free end of the centerline should obey the relation [34]

$$D_\phi = D_{\phi_0} \left[ I_0 \left( \frac{\Delta E}{2k_B T} \right) \right]^{-2}, \quad (15)$$

where  $I_0$  denotes the modified Bessel function of the first kind [33]. The robustness of the scaling  $\sim N^{-5}$  of  $D_\phi$  confirms again that the energy barrier  $\Delta E$  has to be independent of  $N$  for the lengths we considered. To compare the diffusion at different temperatures, we introduce a new scaled (temperature-independent) diffusion coefficient  $\tilde{D} = \frac{D_\phi}{k_B T} \left[ I_0 \left( \frac{\Delta E}{2k_B T} \right) \right]^2$ .

In Fig. 10 we see that the simulation results for different temperatures collapse to a single curve for  $\Delta E \approx 12.5$ . This coincides again with the previous results. The master curve is slightly below the curve for the perfect rotor diffusion coefficient  $\tilde{D}_{\phi_0}$ .

This small discrepancy can be understood as the polymeric tube is softer than the ideal rigid rotor. Indeed, it has to sustain some additional deformations due to the presence and migration of defects in the confostack. The reaction coordinate between two angular orientations is

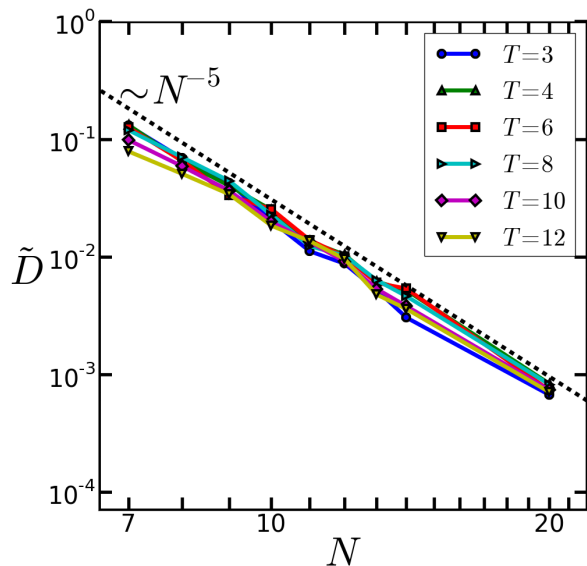


FIG. 10: Scaled diffusion coefficient  $\tilde{D}$  as a function of the number of sections  $N$  of the tube for different temperatures. The  $N^{-5}$  scaling can be explained by the diffusion of a clamped circular arc in a fluid. The collapse of the data on one master curve can only be understood when the internal polymorphic dynamics is properly taken into account (see text).

therefore in reality not straight as it would be for a rigid rotor, but instead the system has to take a non-straight “detour” in the configuration space. This leads to an apparent reduction of the diffusion constant along the ideal (shortest path) rotary reaction coordinate.

To summarize, we have seen that both the external friction of the arc (through the external fluid medium) as well as an internal dissipation mechanism (crossing an inner energetic barrier) of the tube combine together into an effective friction  $\xi_\phi = k_B T / D_\phi$ . Note that contributions of an anomalous friction in the short modes of microtubules were reported by Jansen & Dogterom [35], Taute et al. [32] and Brangwynne et al. [36]. It was speculated by these researchers that some form of internal dissipation mechanism was at work. In this section we have seen how internal barriers and conformational cooperativity give rise to such internal friction phenomena.

## V. CONCLUSION

The elastic and thermal properties of isotropic and anisotropic macromolecular tubes have been the focus of scientific research for decades. In this paper we have studied a new system consisting of a tubular lattice whose individual elements can switch between a flat and a curved configuration. This triggers the birth of “confoplexes”, conformational quasiparticles that interact *via*

long-range repulsive interactions mediated by the elasticity of the lattice. By introducing structural cooperativity (as motivated by biological systems) and in turn “polymerizing” a number of confoplexes on the tubular lattice, a plethora of different phenomena have been discovered: the tube spontaneously breaks its cylindrical symmetry and forms superhelical structures in three-dimensional space. Remarkably, at finite temperature, the movement of the quasipolymer built out of confoplexes on the lattice constantly reshapes the whole tube inducing a random rotation for a clamped tube. This dynamics has been studied in detail by numerical simulations and phenomenological theory. We found that the quasipolymer—the confostack—has to cross a periodic energy barrier to move azimuthally on the lattice. We observe that the typical conformational mode for barrier crossing is a conformational defect that we termed a confostack-kink. The associated kink-dynamics of the confostack on the lattice was the clue to explain the behavior of the diffusion coefficient of the clamped tube.

Looking back at what we have learned from the present tube model, we note one interesting perspective crystallizing out. It is the idea of localized conformational quasiparticles living on the lattice. We have seen how an elementary quasiparticle—the confoplex—emerges and how it interacts with others of the same kind via elastic lattice modes. Once an additional cooperative interaction is introduced, the particle-like confoplexes are forced together into an extended polymer-like conformational object—the confostack. However, curiously the quasipolymeric confostack tends, once again, to decompose into smaller discrete entities. This gives rise to another discrete localized particle-like entity—the confostack-kink.

Exploring the implications of the quasiparticle point of view to study the “confotronics” of a multitude of concrete biological (tubular or cylindrical) monomer lattices, like flagellin, microtubules and actin, promises quite some excitement ahead.

## Acknowledgments

The PMMS (Pôle Messin de Modélisation et de Simulation) is acknowledged for providing the computer time. We thank Albert Johner, Jean-François Joanny, Carlos Marques, Helmut Schiessel, René Messina and Norbert Stoop for stimulating discussions.

## Appendix A: Details of the simulations

Each vertex of the lattice is treated as a bead subject to the equation of motion:

$$m\ddot{\mathbf{r}} = \mathbf{f} - m\gamma\dot{\mathbf{r}} + \mathbf{\Gamma}, \quad (\text{A1})$$

where  $m$  is the mass of the bead, and  $\gamma$  is the damping constant.  $\mathbf{\Gamma}$  denotes the Gaussian white noise, and  $\mathbf{f}$  is the sum of the (elastic) forces acting on the bead.

The corresponding discrete velocity Verlet algorithm reads [37]

$$\begin{aligned}\dot{\mathbf{r}}_{n+1/2} &= \dot{\mathbf{r}}_n + (\mathbf{f}(\vec{r}_n) - m\gamma\dot{\mathbf{r}}_n + \mathbf{\Gamma}_n) \frac{\Delta t}{2m}, \\ \mathbf{r}_{n+1} &= \mathbf{r}_n + \dot{\mathbf{r}}_{n+1/2} \Delta t, \\ \dot{\mathbf{r}}_{n+1} &= \dot{\mathbf{r}}_{n+1/2} + (\mathbf{f}(\vec{r}_{n+1}) - m\gamma\dot{\mathbf{r}}_{n+1} + \mathbf{\Gamma}_{n+1}) \frac{\Delta t}{2m},\end{aligned}\quad (\text{A2})$$

where the noise term is sampled with zero mean and a variance  $\langle \Gamma_i^2 \rangle = 2k_B T_0 m \gamma / \Delta t$  for each component  $i$  with room temperature  $T_0$ . In the simulations, we set the Boltzmann constant, the mass and the damping coefficient to unity. The integration time step is set to  $\delta t = 0.001 \tau$ , where  $\tau$  denotes the unit of time in the simulations.

The elastic parameters in the simulations are chosen in the following manner: The rest lengths are set to  $d_1^{(0)} = d_2^{(0)} = d_3^{(0)} = d$  and  $d_4^{(0)} = \sqrt{2}d$ , where  $d = 4 \text{ nm}$  is the size of a monomer, chosen as the unit length of the system. The angular constants are given by  $s_1^{(0)} = s_4^{(0)}$  and  $s_3^{(0)} = \sin \frac{2\pi}{13}$ . These values ensure that the lattice is cylindrical in the absence of the anharmonic potential.

The value of the stretching rigidity  $\mu_s$  is specified in the main text. For the diagonal bonds, we apply  $\mu_{s4} = 1000 k_B T_0 / d^2$  which is sufficient to conserve the rectangular nature of the subunits. A bending rigidity  $\mu_{b4} = 500 k_B T_0$  is chosen for the diagonal bonds. The bending rigidity of the bonds  $B_3$  is set to  $\mu_{b3} = 1500 k_B T_0$ .

The coefficients of the anharmonic bending potential  $E_2^{\text{BAH}}$  of the bonds of type  $B_2$ , given in Eq. (3), are set to  $A = 3350 k_B T_0$ ,  $B = 2960 k_B T_0$ ,  $C = 290 k_B T_0$  to ensure that  $\Delta G = 200 k_B T_0$  and  $\delta G = 1 k_B T_0$ . The global minimum of  $E_2^{\text{BAH}}$  is situated at  $\bar{s}_2 = -0.588$ . This value leads to a preferred curved state with an angle  $36^\circ$  of the free dimer. Note that, if we approximated the double well potential by a harmonic one around  $\bar{s}_2$ , we could write  $E_2^{\text{BAH}} \approx \frac{\mu_{b2}}{2} \sum_{\{s_2\}} (s_2 - \bar{s}_2)^2$  with an effective bending rigidity  $\mu_{b2} \approx 2000 k_B T_0$ , a value slightly larger than  $\mu_{b3}$ .

### Appendix B: Rigid rotor dynamics in a surrounding fluid

To explain the temporal diffusion of the clamped polymorphic tube, we need the diffusion coefficient of a rotating rigid circular arc in a fluid. Assuming a constant friction per unit length for the cross section of the arc,  $\xi_\perp$ , the Rayleigh dissipation functional is given as  $P_{\text{diss}} = \frac{1}{2} \xi_\perp \int_0^L \dot{\rho}(s, t)^2 ds = \frac{1}{2} \xi_\perp \int_0^L \rho^2 \omega^2 ds$  where  $\omega$  is the angular velocity of the rotor. Since the deflection of the arc is  $\rho(s) = \frac{1}{2} \kappa s^2$ , we obtain  $P_{\text{diss}} = \frac{1}{2} \xi_{\phi_0} \omega^2$  with an effective rotational friction  $\xi_{\phi_0}$  that can be directly read off  $\xi_{\phi_0} = \frac{\xi_\perp \kappa^2 L^5}{20}$ . The azimuthal diffusion coefficient  $D_{\phi_0} = \frac{k_B T}{\xi_{\phi_0}}$  of the free end of the centerline is thus:

$$D_{\phi_0} = \frac{5}{8} \frac{k_B T}{\xi_\perp \kappa^2 d^5} N^{-5} \quad (\text{B1})$$

where  $N = L/(2d)$  (see Sec. IV A 3).

### Appendix C: The emergence of a polymorphic confostack-kink

The wobbling mode of the clamped polymorphic tube is due to the formation of a particular confostack configuration which allows the tube to cross the angular energy barrier. The details of this movement can be understood with the help of a phenomenological model.

The energy of a confostack, Eq. (11), can be written in terms of the transformed angle  $\psi = 13\varphi$  and the scaled polymorphic stiffness  $\tilde{C}_p = 13^{-2} C_p$  as

$$\Delta E(L) = \int_{-L/2}^{L/2} ds \left[ \frac{\tilde{C}_p}{2} \psi'^2 + \frac{W}{2} (1 + \cos \psi) \right]. \quad (\text{C1})$$

This energy has to be minimized with the boundary conditions  $\psi'(\pm L/2) = 0$  (no torque) to find the barrier-crossing configuration of the confostack. This gives the Euler-Lagrange equation

$$\ell^2 \psi'' = -\sin \psi \quad (\text{C2})$$

with  $\ell = \sqrt{2\tilde{C}_p/W}$ . There is always the trivial configuration  $\psi(s) = 0$  with energy  $\Delta E(L) = WL$  and a non-trivial antisymmetric solution with  $\psi(0) = 0$ :

$$\psi(s) = 2 \text{am} \left( \frac{s}{\ell \sqrt{m}}, m \right) \quad \text{with } m = \frac{4}{2+C} \quad (\text{C3})$$

with  $\text{am}(s, m)$  the Jacobi amplitude function of parameter  $m \in [0, 1]$  [33] and  $C$  a constant of integration. The solution describes a revolving pendulum which is a multi-kink solution. A single kink can be defined on a finite region of size  $L$ , given implicitly by the relation  $\sqrt{m} K[m] = L/2\ell$ . However, the boundary conditions  $\psi'(\pm L/2) = 0$  can never be satisfied in this case, except for  $L \rightarrow \infty$  ( $m \rightarrow 1$ ). Nevertheless, a physical solution for a finite length of the confostack can be obtained by analytic continuation of Eq. (C3) choosing  $m > 1$ :

$$\psi(s) = 2 \arcsin \left( \frac{1}{\sqrt{m}} \text{sn} \left[ \frac{s}{\ell}, 1/m \right] \right) \quad \text{with } m > 1. \quad (\text{C4})$$

This solution is a periodic function. It is monotonous on a finite interval given by  $L(m) = 2\ell K[1/m]$ . The associated energy is

$$\Delta E(m) = \frac{\tilde{C}_p}{\ell} \left( 8E[1/m] - \frac{4(m-1)}{m} K[1/m] \right). \quad (\text{C5})$$

with  $K$  and  $E$  being the complete elliptic integrals of the first and the second kind.

For  $m \simeq 1$ , and thus  $L$  very large,  $\psi(s) = 4 \arctan(e^{\frac{s}{\ell}}) - \pi$  and the barrier energy is a constant  $\Delta E \approx 8\tilde{C}_p/\ell$ . Increasing  $m$  decreases  $L$ , and the energy stays close to

its plateau value  $8\tilde{C}_p/\ell$ . When  $L$  approaches  $L_c = \pi\ell$ ,  $\Delta E$  decreases sublinearly and reaches  $\Delta E \approx 2\tilde{C}_p\pi/\ell$  for  $L = L_c$  ( $m = \infty$ ). For  $L < L_c$ ,  $\psi(s) = 0$  is the only

solution, and the barrier scales linearly with  $L$  in this regime. A comparison with the results of the numerical simulations is presented in the main text.

- 
- [1] S. Iijima, *Helical microtubules of grafitic carbon*, Nature **354**, 56 (1991).
- [2] F. Mathieu et al., *Six-Helix Bundles Designed from DNA*, Nano Letters **5**, 661 (2005).
- [3] T. Shimizu, M. Masuda, H. Minamikawa, *Supramolecular Nanotube Architectures Based on Amphiphilic Molecules*, Chem. Rev. **105**, 1401 (2005).
- [4] Y. Yamamoto et al., *Photoconductive Coaxial Nanotubes of Molecularly Connected Electron Donor and Acceptor Layers*, Science **314**, 1761 (2006).
- [5] X. B. Zhang et al., *The Texture of Catalytically Grown Coil-Shaped Carbon Nanotubes*, Europhys. Lett. **27**, 141 (1994).
- [6] A. Volodin, M. Ahlskog, E. Seynaeve, C. van Haesendonck, *Imaging the Elastic Properties of Coiled Carbon Nanotubes with Atomic Force Microscopy*, Phys. Rev. Lett. **84**, 3342 (2000).
- [7] B. I. Dunlap, *Constraints on small graphitic helices*, Phys. Rev. B **50**, 8134 (1994).
- [8] S. M. Douglas, J. J. Chou, W. M. Shih, *DNA-nanotube-induced alignment of membrane proteins for NMR structure determination*, Proc. Natl. Acad. Sci. U.S.A. **104**, 6644 (2007).
- [9] G.-M. Nam et al., *Helices at interfaces*, Europhys. Lett. **100**, 28001 (2012).
- [10] L.-S. Li et al., *A Torsional Strain Mechanism To Tune Pitch in Supramolecular Helices*, Angew. Chem. Int. Ed. **119**, 5977 (2007).
- [11] C. R. Calladine, *Construction of bacterial flagella*, Nature **255**, 121 (1975).
- [12] H. Mohrbach, A. Johner, I. M. Kulić, *Tubulin Bistability and Polymorphic Dynamics of Microtubules*, Phys. Rev. Lett. **105**, 268102 (2010).
- [13] H. Mohrbach, A. Johner, I. M. Kulić, *Cooperative lattice dynamics and anomalous fluctuations of microtubules* Eur. Biophys. J. **41**, 217 (2012)
- [14] L. A. Amos, W. B. Amos, *The bending of sliding microtubules imaged by confocal light microscopy and negative stain electron microscopy*, J. Cell Sci. Suppl. **14**, 95 (1991).
- [15] C. Elie-Caille et al., *Straight GDP-tubulin protofilaments form in the presence of taxol*, Curr. Biol. **17**, 1765 (2007).
- [16] D. Chretien, R. H. Wade, *New data on the microtubule surface lattice*, Biol. Cell. **71**, 161 (1991).
- [17] S. V. Srigiriraju, T. R. Powers, *Continuum Model for Polymorphism of Bacterial Flagella*, Phys. Rev. Lett. **94**, 248101 (2005).
- [18] H. Wada, R. R. Netz, *Discrete elastic model for stretching-induced flagellar polymorphs*, Europhys. Lett. **82**, 28001 (2008).
- [19] B. Friedrich, *A mesoscopic model for helical bacterial flagella*, J. Math. Biol. **53**, 162 (2006).
- [20] A. Goriely, M. Tabor, *Spontaneous Helix Hand Reversal and Tendril Perversion in Climbing Plant*, Phys. Rev. Lett. **80**, 1564 (1998).
- [21] H. Wada, R. R. Netz, *Model for Self-Propulsive Helical Filaments: Kink-Pair Propagation*, Phys. Rev. Lett. **99**, 108102 (2007).
- [22] R. E. Goldstein, A. Goriely, G. Huber, C. W. Wolgemuth, *Bistable helices*, Phys. Rev. Lett. **84**, 1631 (2000).
- [23] I. M. Jánosi, D. Chrétien, H. Flyvbjerg, *Modeling elastic properties of microtubule tips and walls*, Eur. Biophys. J. **27**, 501 (1998).
- [24] H. Mohrbach, I. M. Kulić, *Solvable model for polymorphic biofilaments*, Phys. Rev. E **85**, 031903 (2012).
- [25] H. S. Seung, D. R. Nelson, *Defects in flexible membranes with crystalline order*, Phys. Rev. A **38**, 1005 (1988).
- [26] J. Rudnick, R. Bruinsma, *DNA-Protein Cooperative Binding through Variable-Range Elastic Coupling*, Biophys. J. **76**, 1725 (1999).
- [27] T. R. Weikl, *Indirect interactions of membrane-adsorbed cylinders*, Eur. Phys. J. E **12**, 265 (2003).
- [28] M. M. Müller, M. Deserno, J. Guven, *Geometry of surface-mediated interactions*, Europhys. Lett. **69**, 482 (2005).
- [29] M. M. Müller, M. Deserno, J. Guven, *Interface-mediated interactions between particles: A geometrical approach*, Phys. Rev. E **72**, 061407 (2005).
- [30] S. Mkrtchyan, C. Ing, and J. Z. Y. Chen, *Adhesion of cylindrical colloids to the surface of a membrane*, Phys. Rev. E **81**, 011904 (2010).
- [31] F. Pampaloni et al., *Thermal fluctuations of grafted microtubules provide evidence of a length-dependent persistence length*, Proc. Natl. Acad. Sci. U.S.A. **103**, 10248 (2006).
- [32] K. M. Taute, F. Pampaloni, E. Frey, E.-L. Florin, *Microtubule dynamics depart from the wormlike chain model*, Phys. Rev. Lett. **100**, 028102 (2008).
- [33] M. Abramowitz, I. Stegun, *Handbook of Mathematical Functions*, Dover, New York (1972).
- [34] H. Risken, *The Fokker-Planck Equation: Methods of Solution and Applications*, Springer (1996).
- [35] M. E. Janson, M. Dogterom, *A bending mode analysis for growing microtubules: evidence for a velocity-dependent rigidity*, Biophys. J. **87**, 2723 (2004).
- [36] C. Brangwynne, G. Koenderink, E. Barry, Z. Dogic, F. MacKintosh, D. Weitz, *Bending dynamics of fluctuating biopolymers probed by automated high-resolution filament tracking*, Biophys. J. **93**, 346 (2007).
- [37] T. Schlick, *Molecular Modeling and Simulation: An Interdisciplinary Guide*, Springer (2010).